ELSEVIER

Catalysis Today 70 (2001) 311–320

CATALYSIS TODAY

www.elsevier.com/locate/cattod

Roughening of catalytic surface due to reversible surface reconstruction coupled with oscillatory dynamics: a Monte Carlo study

M. Monine, L.M. Pismen*

Department of Chemical Engineering and Minerva Center for Nonlinear Physics of Complex Systems, Technion, 32000 Technion City, Haifa, Israel

Abstract

Pattern formation processes on single-crystal catalytic surfaces involve transitions between alternative surface phases coupled with oscillatory reaction dynamics. A qualitative Monte Carlo model has been developed in order to describe dynamics of Pt(1 1 0) surface reconstruction under reactive conditions on atomic scale. We use kinetics of a phenomenological time-dependent Ginzburg–Landau (TDGL) type, which is known to give a correct qualitative picture of oscillations. However, the lattice dynamics model involves realistic effects of nearest neighbor interactions dependent on the surface coverage. The surface phase distribution oscillates chaotically together with adsorbate coverage, and, in addition, undergoes a slow roughening process, resulting in the growth of island size and an increase of the oscillation period.

Keywords: Catalytic surface; Surface reconstruction; Oscillatory dynamics; Monte Carlo study

1. Introduction

Catalytic reactions are often accompanied by restructuring of the active surface. A well-studied example is the oxidation of CO on single crystal Pt(1 1 0) surface, where $1 \times 1 \rightarrow 1 \times 2$ reconstruction of clean surface is lifted under the action of adsorbed CO. This produces an autocatalytic effect, leading to oscillatory behavior and pattern formation [1]. The mechanism of complex dynamic behavior based on adsorbate-induced surface phase transitions has been incorporated in a phenomenological kinetic model, which includes the fraction of the surface occupied by one of the alternative phases as one of the dynamic variables [2]. This model provided a realistic (at least in a qualitative sense) picture of kinetic oscillations and pattern formation on the Pt(1 1 0) surface on a micrometer scale, but could not account for more subtle effects requiring higher resolution.

Since both $1 \times 1 \rightarrow 1 \times 2$ reconstruction and its reverse involve mass transport [3], repeated transitions accompanying kinetic oscillations may lead to roughening and faceting of an originally flat surface. This, in turn, may cause slow changes in average catalytic activity observed in the experiment [4], or formation of local patches of modified catalytic activity serving as channels for propagating pulses [5].

Neither roughening nor a related drift of reaction rates can be explained without describing local dynamics of surface phase transitions more mechanistically. On the mean field level, this can be done by assuming that $1 \times 1 \rightleftharpoons 1 \times 2$ transition is carried by propagating fronts [6]. The essence of the model is the assumption

* Corresponding author.
E-mail address: pismen@techunix.technion.ac.il (L.M. Pismen).

0920-5861/01/$ – see front matter
PII: S0920-5861(01)00339-X

that the surface phase transition is a slow local process that leads to the formation of a nanoscale pattern of surface phases, and manifests itself in slow motion of interphase boundaries with a speed dependent on the local value of CO coverage. The CO adsorption causes the surface reconstruction into the 1×1 phase on which an oxygen sticking coefficient is higher. The oxygen adsorption and CO_2 formation reaction are assumed to be fast processes and, thus, limited by the CO induced $1 \times 2 \rightarrow 1 \times 1$ reconstruction. The surface reaction yields CO_2 which desorbs immediately, then the reversible $1 \times 1 \rightarrow 1 \times 2$ reconstruction begins on the adsorbate-free surface. For simplification, the computation will not take into account oxygen adsorption, and use the TDGL kinetic equation, which is known to give a correct qualitative picture of oscillations and pattern formation [6,23]. In the framework of this model, it was conjectured that surface roughening may develop in regions repeatedly traversed by advancing and retreating fronts [7], which may explain formation of local channels with modified catalytic activity.

A more realistic description, incorporating also fluctuations, requires modeling on an atomic scale. A suitable framework is provided by Monte Carlo (MC) computations treating motion of surface atoms explicitly. So far, MC computations have been carried out mainly for studying either equilibrium properties of surfaces or dynamics of surface growth [8–21]. Recent MC computations of surface reconstruction coupled to oscillatory catalytic kinetics did not resolve actual changes of local surface atomic structure, but described the surface phase transition formally as a switch of a site tag.

The aim of this communication is to investigate a basic MC model of formation of surface phase domains and roughening coupled with chemical oscillations. The computation will resolve the surface structure explicitly through motion of Pt atoms between crystal surface sites, while the chemical environment will be modeled by a single global variable coupled to averaged characteristics of the surface. In the case of CO oxidation on Pt, this approach is justified by a large diffusivity of adsorbed CO (which is the main agent affecting the surface reconstruction) compared to Pt. Since at the moment there are no quantitative data on energies of different surface configurations and activation energies of various possible transitions of Pt atoms, we shall compute configuration energies taking into account only the interactions between neighboring atoms, and assign their dependence on the global variable (CO coverage) in such a way as to ensure the desired change of relative energies of the reconstructed and unreconstructed surfaces. Our results will give, therefore, only a qualitative picture of surface restructuring; the method, however, can be readily extended to include more realistic kinetics.

2. The model

We consider a face-centered cubic lattice (FCC). Only atoms occupying top sites (i.e. not covered by any neighboring atom in the higher layer) are allowed to move. Thus, for a patch containing $N \times N$ sites in each layer, we have to keep track of $2N^2$ sites. The sites are numbered in the horizontal plane as shown in Fig. 1. In addition, each site carries an integer tag representing the vertical position of its upper atomic layer $L_{j,i}$. Take note that sites with the index j even or odd lie in adjacent layers. With this choice of labeling, the index j runs from 0 to $2N$, while the index i runs from 0 to N. It is assumed that the atomic structure has no overhangs, i.e. each surface atom $\{j, i\}$ is always based on four occupied sites in the layer below.

The energy of surface atoms is assumed to be dependent on the occupancy of the eight nearest sites in the same layer:

$$\begin{aligned} E_{i,j} = {} & Q_1(S_{i,j-2} + S_{i,j+2}) + Q_2(S_{i+1,j} + S_{i-1,j}) \\ & + Q_3(S_{i+1,j+1} + S_{i+1,j-2} \\ & + S_{i-1,j+2} + S_{i-2,j-2}), \end{aligned} \tag{1}$$

where $S_{i,j} = 1$ for an occupied site and $S_{i,j} = 0$ for a vacant one, and Q_k are interaction energies. A similar form for a surface Hamiltonian has been proposed in Ref. [22]. The difference between Q_1 and Q_2 accounts for the anisotropy of a (1 1 0) plane, while both energies are equal for a (1 0 0) surface. In some computations, interaction with the next nearest sites was also taken into account, which has not affected the results in a qualitatively significant way.

Positive Q_3 makes 1×2 reconstruction energetically favorable, whereas the 1×1 structure becomes preferred when Q_3 decreases. The 1×2 configuration of a clean Pt(1 1 0) surface is preferable, because the

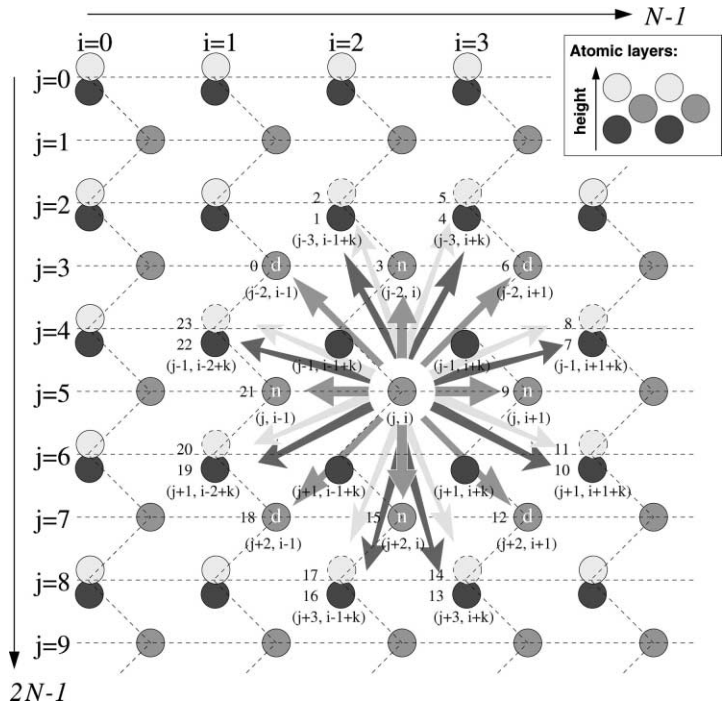

Fig. 1. A scheme of the surface lattice. For a given atom with $\{j, i\}$, 24 new possible positions are determined by combination of indices. The index shift k is determined as $k = j - 2\,\mathrm{Int}(j/2) = \{0\,\text{for even}\,j;\ 1\,\text{for odd}\,j\}$. (NB: a unit surface cell in the (1 1 0) plane has a rectangle form with the $\sqrt{2}$ aspect ratio; this scale ratio is not preserved in this and other drawings.)

surface energy of the 1×2 row atoms is lower compared to that of a more close-packed 1×1 configuration. The CO adsorption destabilizes the 1×2 state favoring the 1×1 structure. This can be modeled by making Q_3 a decreasing function of the surface averaged CO coverage θ. We shall also allow Q_2 to be θ-dependent, while Q_1 will be kept constant. Thus, we assume the following coverage dependence of the interaction energies:

$$Q_1 = -q_1, \qquad Q_2 = -q_2(\theta - c_2),$$
$$Q_3 = q_3(1 - \theta). \tag{2}$$

The values used in the following computations are $q_1 = 0.3\,\mathrm{eV}$, $q_2 = 0.4\,\mathrm{eV}$, $c_2 = 0.25\,\mathrm{eV}$, $q_3 = 0.08\,\mathrm{eV}$.

The coupling to chemical kinetics is modeled by the equation for a global variable v of the same form as in Ref. [6]:

$$\gamma^{-1} v_t = v - v^3 - \eta, \tag{3}$$

where γ is the time-scale ratio. The variable v models action of the CO adsorbate lifting the $1 \times 2 \to 1 \times 1$ reconstruction and plays a role of "fast activator". The oxygen coverage is slaved to the CO coverage and, therefore, its action is not included explicitly. Eq. (3) has two stable stationary states biased by the level of a "slow inhibitor" η, which is defined here in such a way that the level $\eta = 0$ corresponds to the Maxwell construction. We interpret it here as a surface state variable that models the inhibiting action of the 1×2 reconstruction. The correspondence to the surface structure and coverage is established through the relations

$$v = \frac{2}{\sqrt{3}}(2\theta - 1) \quad \text{and} \quad \eta = a(\theta_{\mathrm{top}} - b)$$

with $a = 2.333$ and $b = 0.68$. The first relation maps the two stationary states of Eq. (3) onto the low- and high-coverage states (respectively, for v negative and positive). The second relation models the feedback of the surface structure by introducing a bias in favor of

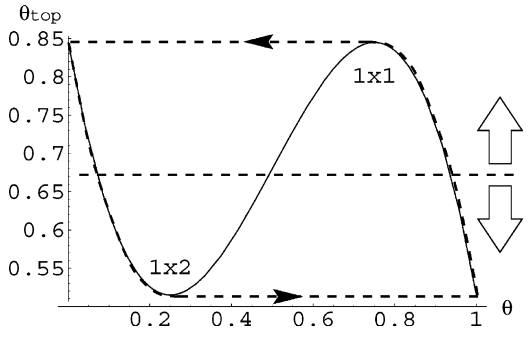

Fig. 2. The nullcline of Eq. (3) in the (θ, θ_{top}) plane.

the low-coverage state when the fraction of free top sides θ_{top} is high and in favor of the high-coverage state when the θ_{top} is low. The model variables θ and θ_{top} are averaged over the entire surface which is reproduced by the lattice of $2N^2$ sites. Such averaging can be justified by the fact that CO diffuses more rapidly than Pt adatoms within the simulated area.

Since θ_{top} changes from 0.5 for the 1×2 configuration to 1 for an ideal 1×1 surface, transition to the 1×1 state favors the low-coverage state of Eq. (3). This, in turn, causes surface reconstruction, leading to a decrease of η and transition to the high-coverage state. Fig. 2 illustrates a nullcline of Eq. (3) and hysteretic relaxation between the two states. This models the basic mechanism of oscillations and pattern formation, which acts qualitatively in the same way as in the model of [2] containing two long-range variables.

3. The algorithm

The solution method combines application of the importance sampling MC algorithm to a nano-domain of Pt(1 1 0) surface (simulating the $1 \times 1 \rightleftharpoons 1 \times 2$ reconstruction) with integration of the global equation of the global variable (3).

The transition probabilities for surface atoms are calculated according to the Metropolis rule [24]:

$$W_i = \min\left\{\nu_0 \exp\left(-\frac{\Delta E_i}{k_{\text{B}}T}\right), 1\right\}, \tag{4}$$

where ΔE_i is the energy difference between the new and old positions, k_{B} the Boltzmann constant (eV/K), T the temperature and ν_0 a scaling factor. This rule takes into account only equilibrium energies of surface configurations, which can be computed using Eq. (1) or any other local rule. Activation energies are not taken into account, which actually implies that all possible transitions are assumed to have identical activation energies.

The MC algorithm shifts the atoms between lattice nodes according to the following rules:

1. A random free (not covered by any atom in the higher layer) atom is selected on the lattice.
2. For the chosen free atom, possible jump sites are determined according to the scheme shown in Fig. 1. Any atom can jump only to a free adjacent position in the same layer, or to a neighboring position in the layer above or below, provided this

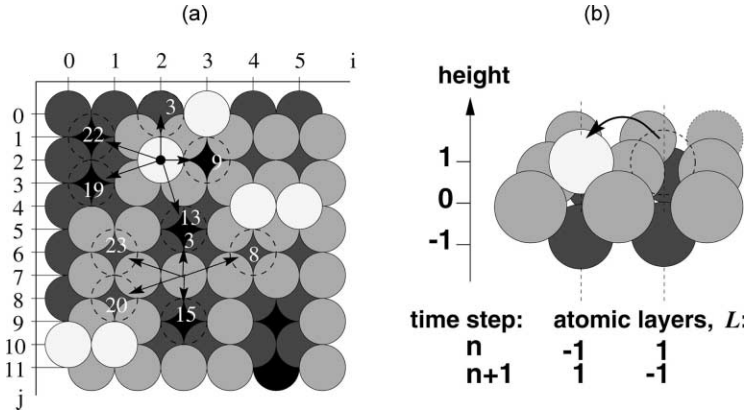

Fig. 3. (a) Possible new positions. (b) Change of the atomic layer tag L at two lattice nodes associated with one step.

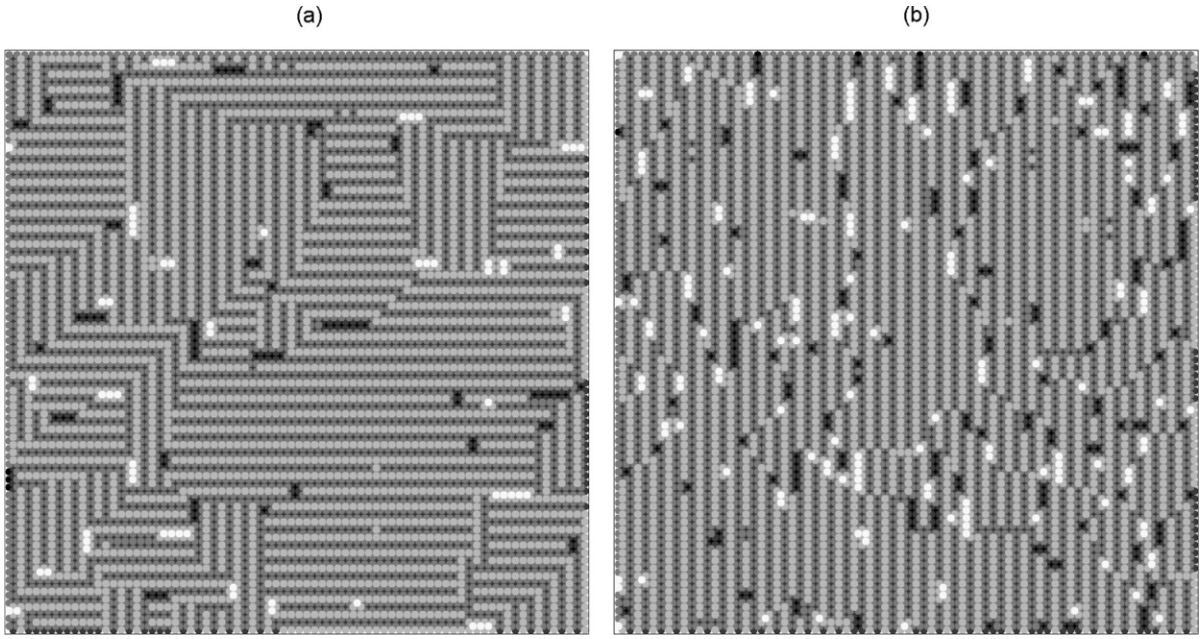

Fig. 4. Missing row structure obtained from random initial conditions. The lattice dimension is $2N^2 = 2 \times 75 \times 75 = 11{,}250$. (a) (1 0 0) surface: $E_{n,\mathrm{vert}} = E_{n,\mathrm{hor}} = -0.3\,\mathrm{eV}$, $E_{nn} = -0.3\,\mathrm{eV}$, $E_d = 0.5\,\mathrm{eV}$; (b) (1 1 0) surface: $E_{n,\mathrm{vert}} = -0.3\,\mathrm{eV}$, $E_{n,\mathrm{hor}} = 0.1\,\mathrm{eV}$, $E_{nn} = -0.3\,\mathrm{eV}$, $E_d = 0.5\,\mathrm{eV}$.

new position is based on four corner atoms of the lower layer. Periodic boundary conditions are applied at the grid boundaries:

$$\{-J, i\} = \{2N - J, i\}, \quad \{2N + J, i\} = \{J, i\},$$
$$\{j, -I\} = \{j, N - I\}, \quad \{j, N + I\} = \{j, I\},$$

where $j = 0, 1, \ldots, 2N-1$ and $i = 0, 1, \ldots, N-1$. Twenty-four possible positions have to be checked, but the number of vacant sites never exceeds 8. An example of enumeration of possible positions is shown in Fig. 3a.

3. The energies of the current and each possible new positions are computed, and the transition probabilities W_i associated with each possible step are computed using Eq. (4) based on the respective energy differences ΔE_i (when the energy at a new site is computed, the old site is assumed to be vacant).

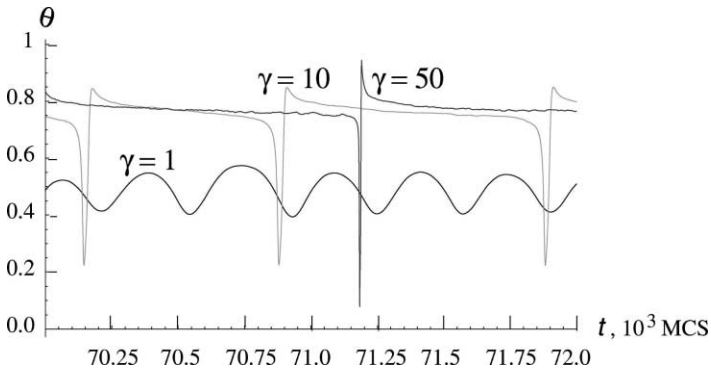

Fig. 5. Comparison of oscillations shape at different γ.

(For more details on steps 2 and 3, see Appendix A.)

4. A random number F uniformly distributed between zero and unity is drawn, and a new position is chosen randomly among the available vacant sites with $W_i > F$ (another option is to select a new position among the sites with $W_i = W_{\max} > F$ if there are a number of possible positions with the same maximal probability $W_{\max}$). If $W_i < F$, the step is not accepted and the calculation returns to step 1.
5. After a new position is selected, the atom is removed from the old position, i.e. the layer tag of the respective site is reduced by 2; the layer tag of the new site is increased by 2 (see Fig. 3b), and the computation returns to step 1.

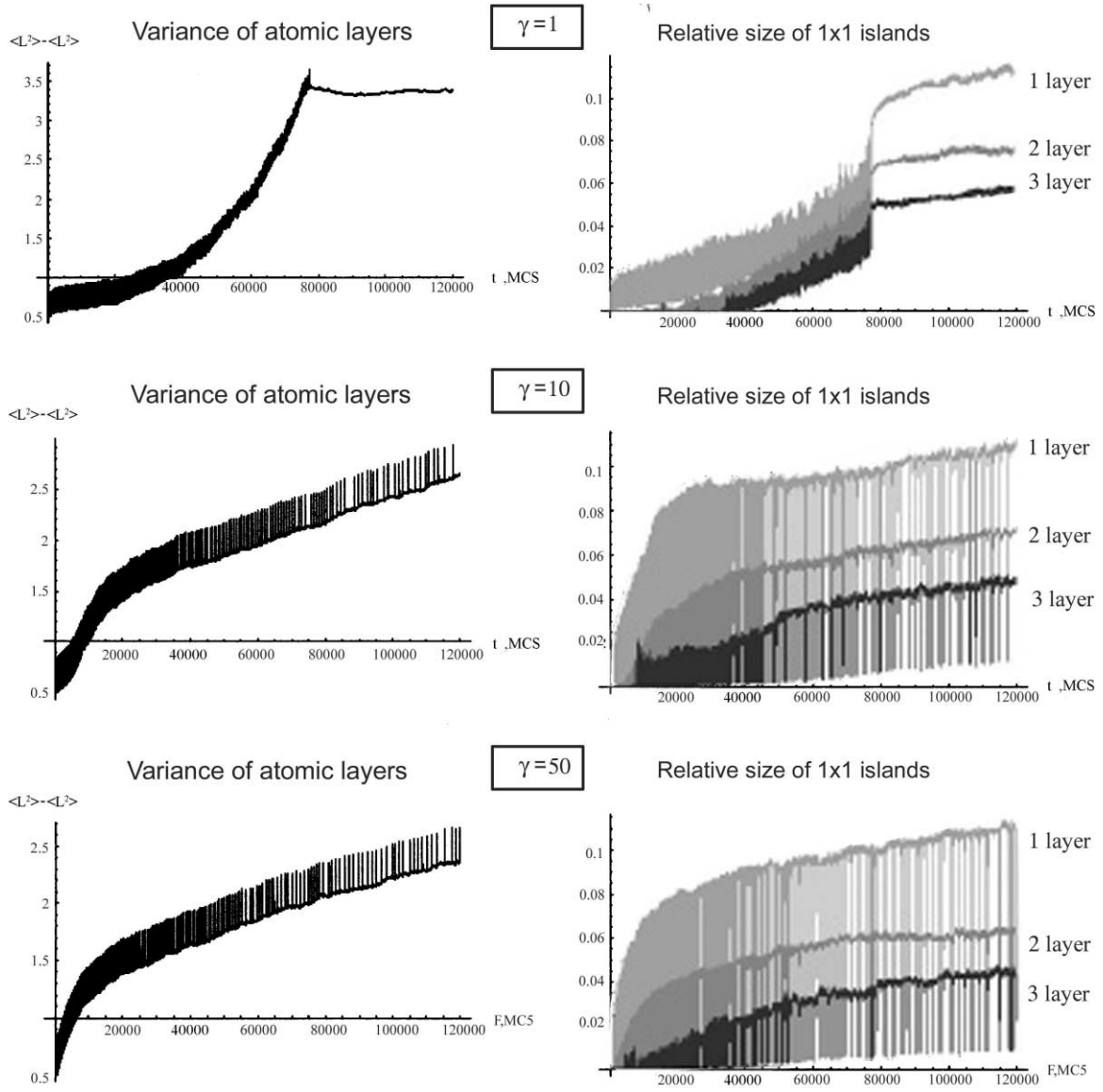

Fig. 6. The variance of the surface atomic layers and relative size of the 1×1 islands on the 1st, 2nd and 3rd layers.

After each MC step (MCS) comprising $2N^2$ moves (the lattice dimension), the numerical data are collected: lattice layers area and variance, fractions of the surface phases, number of top sites, relative size of domains, etc. Eq. (3) is integrated at each MCS.

4. Results and discussion

We take as initial conditions a perfect 1×1 plane randomly covered partially filled upper layer. Fig. 4 shows the results of a test computation at $v = \text{const.}$ with the energy parameters Q_i set in such a way that the 1×2 surface configuration is stable. If $Q_1 = Q_2$ (1 0 0 surface), four types of domains are formed, with the missing rows in both perpendicular directions and a shift by one row for each orientation (Fig. 4a). An anisotropic (1 1 0) surface is more appropriately described by the computation shown in Fig. 4b, carried out with $Q_1 = 0.1\,\text{eV}$ and $Q_2 = -0.3\,\text{eV}$. Here a definite missing rows' orientation characterized by a lower surface energy is established, and there are only two alternative kinds of domains differing by a row shift.

Formation of phase domains has also been observed in the computations coupling the MC algorithm with the equation of the global variable (3), which constitute the principal result of this communication. At the chosen values of the energy parameters, the $1 \times 1 \rightleftharpoons 1 \times 2$ reconstruction is usually initiated at the domain boundaries, atomic steps or defects. This causes slow surface roughening in the course of oscillations.

The time ratio γ is responsible for the adsorption and reaction kinetics rate. Varying this parameter influences the roughening process and oscillatory dynamics in a most spectacular way. Oscillations at $\gamma = 1$ are characterized by slow transition between the 1×1 and 1×2 states, which fails to be completed within an oscillation period (Fig. 5). The oscillation period gradually increased with time, and eventually the oscillations stop. Further surface roughening, expressed both by the variance of the surface atomic layers and by the island sizes (Figs. 6 and 7), almost comes to a halt once oscillations cease.

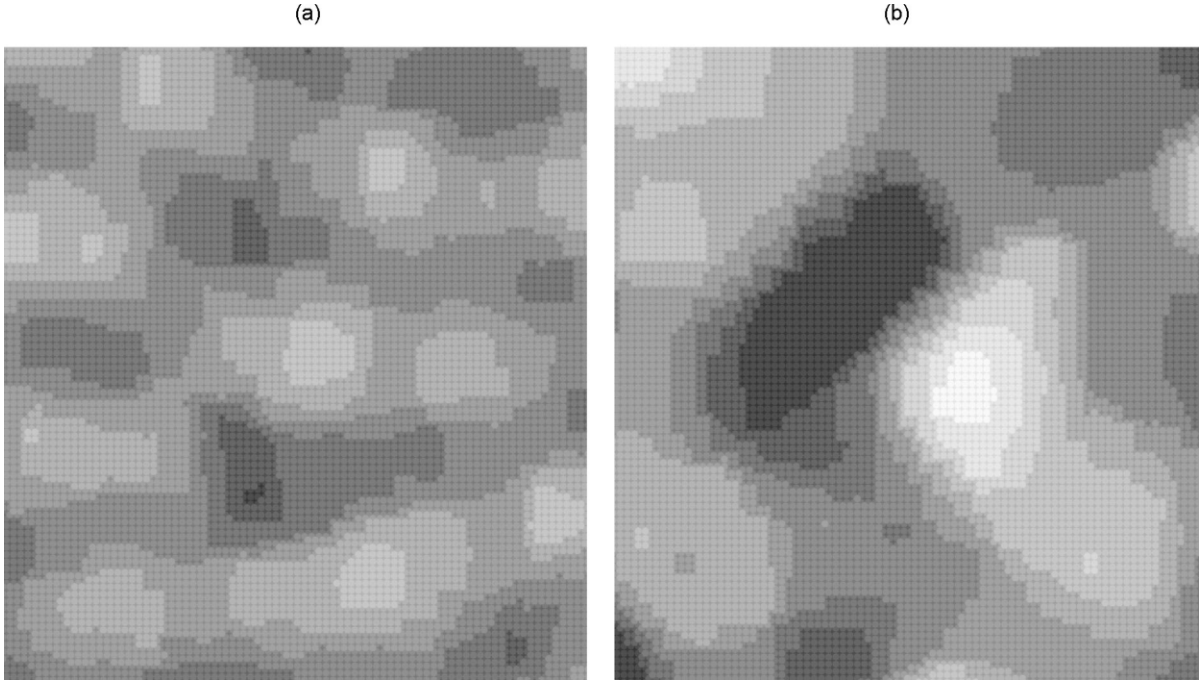

Fig. 7. Top view of two grayscale frames of the same surface fragment at different time moments ($\gamma = 10$). (a) $t = 50 \times 10^3$ MCS, $-4 \le L \le 3$; (b) $t = 350 \times 10^3$ MCS, $-5 \le L \le 5$. The whole simulation area contains $2 \times 150 \times 150$ surface atoms. For simplicity of presentation, the lattice is shown with square unit cells (the $[1\,\bar{1}\,0]$ axis corresponds to the vertical direction).

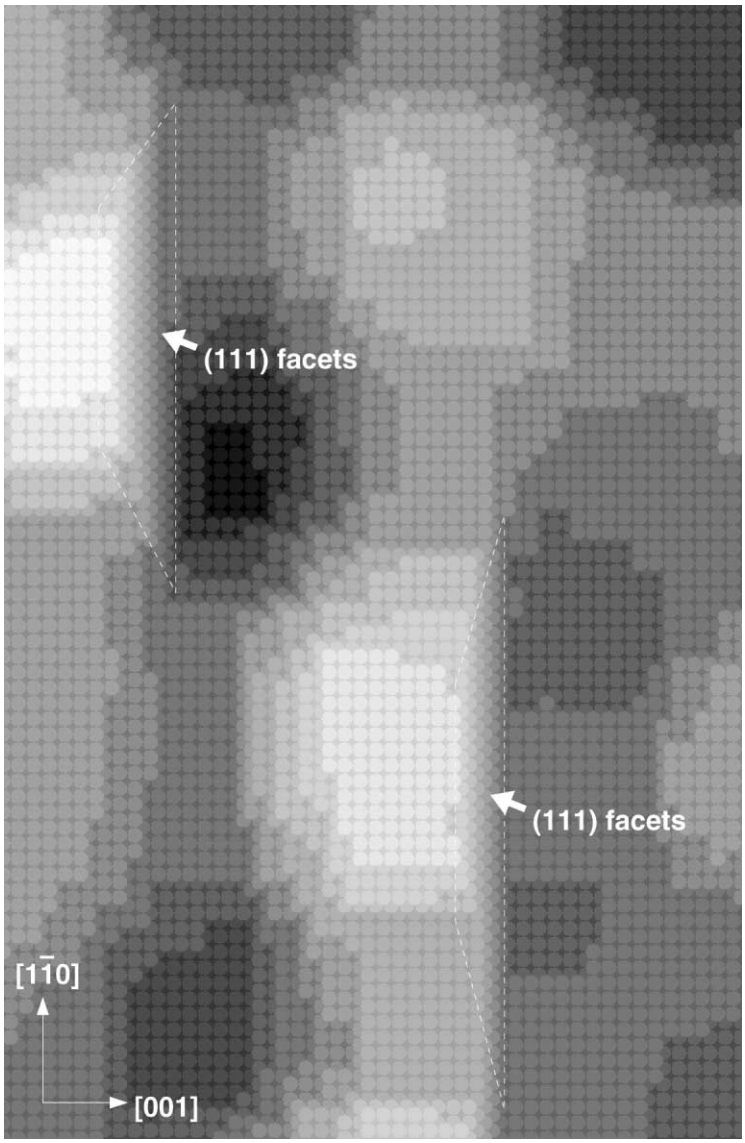

Fig. 8. Fragment of simulation on the $2 \times 150 \times 150$ lattice obtained at $\gamma = 1$ ($t = 1.2 \times 10^5$ MCS). Non-reconstructed (1 1 1) facets are shown.

Numerical results with $\gamma = 10$ and 50 display a different kind of behavior. Transitions between alternative states are fast, and are completed at early stages of each oscillation cycle, leading to a sharp (relaxation-like) shape of coverage oscillations (Fig. 5). The oscillation period tends to grow with time, alongside with increasing roughening and domain size (Figs. 6 and 7). However, the length of each reconstruction period strongly fluctuates so that oscillations are of chaotic character.

At the slow reaction rate ($\gamma = 1$), a more ordered surface structure of pyramid-shaped hills has been obtained (Fig. 8). The pyramid sides oriented along [1 $\bar{1}$ 0] direction form stable (1 1 1) facets which do not reconstruct and, therefore, oscillations are stopped. In contrast, the fast rate (at high γ) causes more rapid

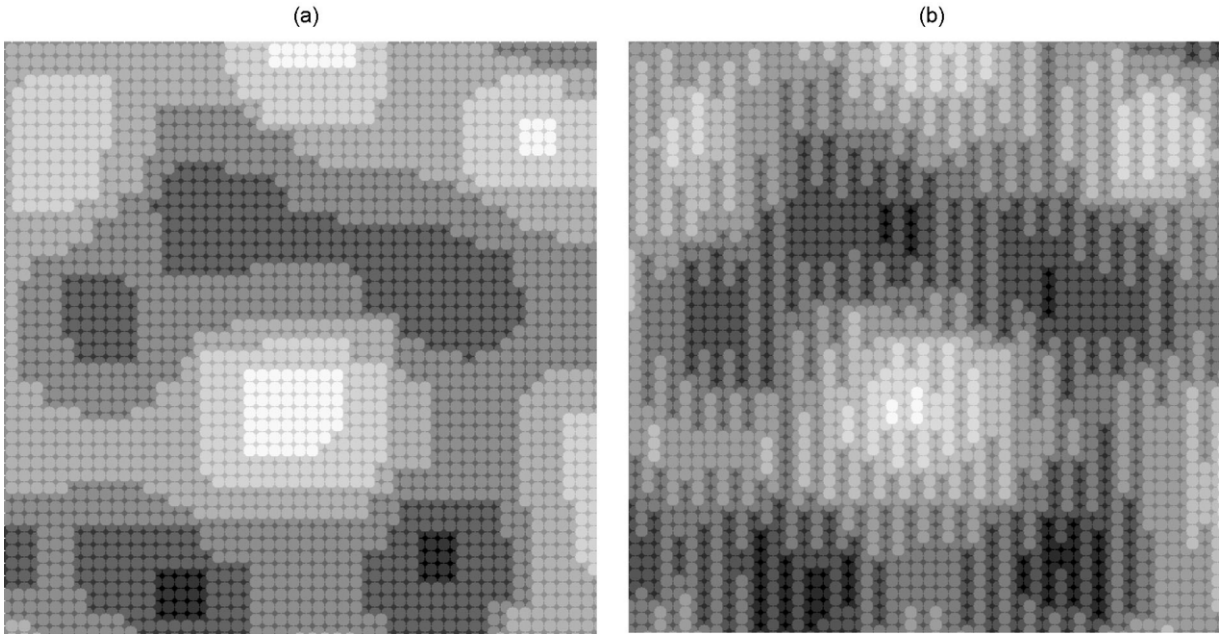

Fig. 9. A typical simulated transition from the 1×1 phase (a) to the 1×2 phase (b). The reconstruction begins at boundaries of the 1×1 domains. For simplicity of presentation, the lattice is shown with square unit cells (the $[1\,\bar{1}\,0]$ axis corresponds to the vertical direction).

and chaotic reconstruction, and roughening process is observed in the course of oscillations.

Fig. 9 illustrates the common mechanism of the $1 \times 1 \rightleftharpoons 1 \times 2$ reconstruction. When θ relaxes towards the lower level, a finger-like growth of the 1×1 nano-domain boundaries begins. The quantity of top atoms decreases as the 1×2 state spreads, until θ relaxes to the upper level and the reverse reconstruction to the 1×1 state starts. The 1×1 state prevails during a longer time compared to the 1×2 phase. Fig. 7 shows grayscale images of 1×1 nano-domains (bright islands) growing via oscillations.

The increase of the oscillation period accompanying growing surface roughness fits the experimental observations [4].

5. Conclusions

The results of the numerical simulations are in good qualitative agreement with the predicted scenario of surface evolution in the $CO_{ad} + O_{ad}/Pt(1\,1\,0)$ reaction [1,9]. The simulation results clearly demonstrate the mechanism of surface roughening and drift and kinetic characteristics caused by repeated $1 \times 1 \rightleftharpoons 1 \times 2$ reconstruction accompanying kinetic oscillations. Roughening is initiated at boundaries of phase domains, and the depth of the surface relief and domain size slowly grow with time. This, in turn, causes an increase of the average oscillation period. Application of the developed algorithm to a model with realistic chemical kinetics requires more data on lattice energies in different environments, and will be a subject of further research.

Acknowledgements

This research has been supported by the German-Israeli Science Foundation.

Appendix A. Computation of all possible transitions

We will enumerate the transitions by either the indices (e.g. $\{j, i\}$ for a randomly chosen atom and $\{m, n\}$ for its nearest neighboring sites) or labels (l) according to Fig. 1. We define eight sets, each of them describing three new possible positions: in the same

layer $L(l)$, in the layer below $L(l+1)$ and in the layer above $L(l+2)$, see Fig. 1. Here the position's label l runs from 0 to 23 with the step 3.

The switch function $B(l)$ describes the availability of neighboring positions with indices $\{m, n\}$ and index shift k determined as

$$k = j - 2\,\mathrm{Int}\left(\frac{j}{2}\right) = \begin{cases} 0 & \text{for even } j, \\ 1 & \text{for odd } j, \end{cases}$$

see Fig. 1. If the following equality

$$\begin{aligned} L_{m,n} &= L_{m-1,n-1+k} - 1 = L_{m+1,n-1+k} - 1 \\ &= L_{m-1,n+k} - 1 = L_{m+1,n+k} - 1 \end{aligned}$$

is true, then $B(l) = 1$, i.e. four corner atoms (base) form a rectangle cell providing a vacant top site. If this equality is not satisfied, then $B(l) = 0$, i.e. there is no base for a top site.

We proceed a loop for l running from 0 to 23 as $l = l + 3$:

1. if $L(l) = L_{j,i}$ and $B(l+2) = 1$, calculate W_{l+2} and store it with the corresponding new *upper* position label $l + 2$;
2. if $L(l) = L_{j,i} - 2$ and $B(l) = 1$, calculate W_l and store it with the corresponding new position label l for *the same* layer;
3. if $L(l) = L_{j,i} - 2$ and $B(l + 2) = 1$, calculate W_{l+1} and store it with the corresponding new *lower* position label $l + 1$.

Note that these three conditions are exclusive and only one of them may be satisfied at each loop.

After this stage, the set of possible new positions l with appropriate transition probabilities W_l is collected.

References

[1] R. Imbihl, G. Ertl, Chem. Rev. 95 (1995) 697.
[2] K. Krischer, M. Eiswirth, G. Ertl, J. Chem. Phys. 96 (1992) 9161.
[3] T. Gritsch, D. Coulman, R.J. Behm, G. Ertl, Phys. Rev. Lett. 63 (1989) 1086.
[4] R. Imbihl, Mod. Phys. Lett. B 6 (1992) 493.
[5] K.C. Rose, B. Berton, R. Imbihl, W. Engel, A.M. Bradshaw, Phys. Rev. Lett. 79 (1997) 3427.
[6] L.M. Pismen, R. Imbihl, B.Y. Rubinstein, M. Monine, Phys. Rev. E 58 (1998) 2065.
[7] L.M. Pismen, B.Y. Rubinstein, Chaos 9 (1999) 55.
[8] V. Zhdanov, Surf. Sci. 426 (1999) 345.
[9] R. Imbihl, A.E. Reynolds, D. Kaletta, Phys. Rev. Lett. 67 (1991) 275.
[10] V. Zhdanov, B. Kasemo, Phys. Rev. E 61 (2000) R2184.
[11] V. Zhdanov, B. Kasemo, J. Stat. Phys. 101 (2000) 631.
[12] H. Park, S. Lee, Surf. Sci. 441 (1998) 1.
[13] M. Kotrla, J. Krug, P. Smilauer, Phys. Rev. B 62 (2000) 2889.
[14] J.J. Lukkien, J.P.L. Segers, P.A.J. Hilbers, R.J. Gelten, A.P.J. Jansen, Phys. Rev. E 58 (1998) 2598.
[15] R.J. Gelten, A.P.J. Jansen, R.A. van Santen, J.J. Lukkien, J.P.L. Segers, P.A.J. Hilbers, J. Chem. Phys. 108 (1997) 5921.
[16] V.N. Kuzovkov, O. Kortluke, W. von Niessen, J. Chem. Phys. 108 (1997) 5571.
[17] X.-G. Wu, R. Kapral, Physica A 188 (1992) 284.
[18] H. Rose, H. Hempel, L. Schimansky-Geier, Physica A 206 (1994) 421.
[19] J.P. Boon, D. Dab, R. Kapral, A. Lawniczak, Phys. Rep. 273 (1996) 55.
[20] A.P.J. Jansen, R.M. Nieminen, J. Chem. Phys. 106 (1997) 2038.
[21] J.P. Hovi, A.P.J. Jansen, R.M. Nieminen, Phys. Rev. E 55 (1997) 4170.
[22] G. Mazzeo, G. Jug, A.C. Levi, E. Tosatti, Phys. Rev. B 49 (7625) 1993.
[23] M. Bär, M. Hildebrand, M. Eiswirth, M. Falcke, H. Engel, M. Neufeld, Chaos 4 (1994) 499.
[24] K. Binder, D.W. Heermann, Monte-Carlo Simulation in Statistical Physics, 2nd Edition, Springer, Berlin, 1992.